Supporting Information

Molecular photo-switches mediating the strain-driven disassembly of supramolecular tubules

Jean W. Fredy[a,b§], Alejandro Méndez-Ardoy[a§], Supaporn Kwangmettatam[a,b§], Davide Bochicchio[c], Benjamin Matt[b], Marc C. A. Stuart[d], Jurriaan Huskens[a], Nathalie Katsonis[b], Giovanni M. Pavan[c*] and Tibor Kudernac[a*]

[a] Molecular Nanofabrication Group, MESA+ Institute for Nanotechnology, University of Twente, PO Box 207, 7500 AE Enschede, The Netherlands.

[b] Bio-inspired and Smart Materials, MESA+ Institute for Nanotechnology, University of Twente, PO Box 207, 7500 AE Enschede, The Netherlands.

[c] Department of Innovative Technologies, University of Applied Sciences and Arts of Southern Switzerland, Galleria 2, Via Cantonale 2c, CH-6928 Manno, Switzerland

[d] Faculty of Mathematics and Natural Sciences, Groningen Institute of Biomolecular Sciences and Biotechnology, University of Groningen, Nijenborgh 7, 9747 AG Groningen, The Netherlands.

[§] These authors contributed equally

* Correspondence to: t.kudernac@utwente.nl, giovanni.pavan@supsi.ch

Table of Contents

1. General methods

Materials. Reagents and solvents were purchased from commercial sources and used without further purification unless stated otherwise. ^{1}H and ^{13}C NMR were recorded at 400 and 100.6 MHz, respectively. 2D COSY and HMQC experiments were used to assist on NMR peak assignments. Chemical shifts are reported in δ = units (ppm) relative to the residual protonated solvent signals of $CDCl_3$ (^{1}H NMR: δ = 7.26 ppm) and CD_3CN (^{1}H NMR: δ = 1.94 ppm). Thin-layer chromatography (TLC) was carried out using Merck silica gel 60 on aluminum sheet, with visualization by UV light and by charring with a potassium permanganate solution (2%) and sodium hydrogen carbonate (4%) in water. Column chromatography was carried out using Merck silica gel 60 (230-400 Mesh). ESI-MS spectra were obtained for samples dissolved in DCM-MeOH at low μM concentrations.

UV-visible and circular dichroism (CD) spectroscopy. The solutions were prepared with concentrations in the micromolar range, at least 18 hours before the irradiation experiments, from a concentrated stock solution in water. All solutions were kept in the dark at all times. UV-visible spectra were recorded at room temperature with a Perkin Elmer Lambda 850 UV-visible spectrometer in 1-cm quartz cells. CD spectra were recorded with a Jasco J-1500 spectrometer. For experiments in water/acetonitrile, acetonitrile was added to a solution of the molecules in water, before irradiation.

Determination of critical aggregation concentrations. Critical aggregation concentrations were determined following a reported procedure (1). Briefly, Nile Red at a concentration of 0.94 μM in milliQ water was used as a fluorescent probe. Dilutions of **1** and **2** were prepared in dye solution and incubated at room temperature for at least 15 min. Fluorescence emission spectra between 580-720 nm were recorded using a fluorescence spectrophotometer (Perkin Elmer LS55) using an excitation at λ = 550 nm.

Dynamic Light Scattering. The samples were prepared a day prior to the acquisition. UV irradiated samples were measured immediately after the irradiation has stopped. DLS measurements were carried out using a Nanotrac (Anaspec) particle analyzer. For each condition, five measurements of 120 s were performed, with a set-zero time of 180 s. Data was analyzed assuming a refractivity index of 1.45. Measurements were carried out at a concentration 80 μM. Particle size was determined following the intensity distribution.

Cryo-TEM. The solutions were prepared by solubilizing the compounds in deionized water at 1.33 mM, one day before the acquisition of micrographs. These solutions were used directly after irradiation. The cryo-TEM samples were prepared by depositing a few microliters of these solutions on carbon-coated grids (Quantifoil 3.5/1, Quantifoil Micro Tools, Jena, Germany). After blotting the excess liquid, the grids were vitrified in liquid ethane (Vitrobot, FEI, Eindhoven, The Netherlands) and transferred to a Philips CM 120 microscope equipped with a Gatan model 626 cryo-stage operating at 120 kV. Micrographs were recorded under low-dose conditions with a slow-scan CCD camera. The highest density is obtained from the electron dense aromatic part of the building blocks.

Transmission electron microscopy (TEM). The samples were prepared by drop-casting 80 μM water solutions on carbon grids (Formvar/Carbon 200 mesh, Copper). Prior to measurements the samples were stained by Uranyl acetate. TEM micrographs were recorded using a Philips CM300ST - FEG microscope.

Atomic force microscopy (AFM). The samples were prepared by drop casting a solution of tubules in water, on freshly cleaved mica. After blotting the excess liquid, the samples were dried in air several hours

and characterized by in tapping mode (Nanoscope IV). The AFM images were analyzed with the LA 1730 software.

Measurements of the diameter and length of the tubules. The Image J 1.46 software was used to analyze AFM images and (cryo-)TEM micrographs. Manual analysis led to determination of the length and diameter of the tubules. Longer tubules are underrepresented as their length was measured only within the size of the micrographs at the suitable magnification.

Irradiation experiments. The samples were irradiated by using a bluepoint LED Hoenle Technology lamp (300 mW.cm^{-2}, λ = 365 nm).

2. Synthesis and characterization

Compounds **1** and **2** were synthesized according to a **Scheme 1**. Compounds **3** (2), **6** (3) and **7** (4) were synthesized according to reported procedures.

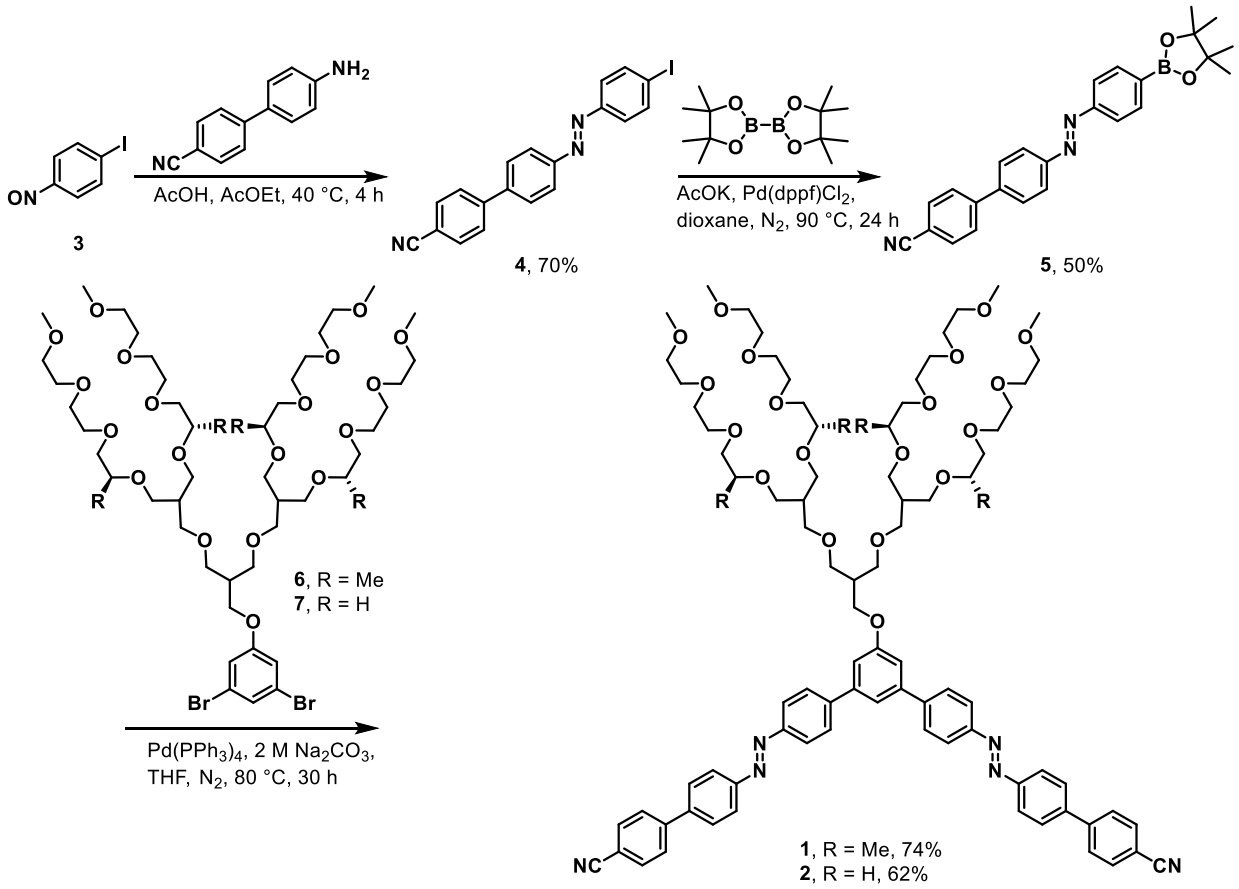

Scheme 1. Synthetic route towards 1 and 2.

(*E*)-4'-((4-iodophenyl)diazenyl)-[1,1'-biphenyl]-4-carbonitrile (4). 4'-Aminobiphenyl-4-carbonitrile (87 mg, 0.45 mmol, 1 eq.) and **3** (105 mg, 0.45 mmol) were dissolved in acetic acid-EtOAc 1:1 (4 mL). The reaction mixture was stirred at 40 °C and an orange solid was formed after 20 min. The reaction was stirred

for 5 h. The precipitated compound was filtered and washed with water, then re-dissolved in dichloromethane, dried over Na_2SO_4, and concentrated to give **4**. Yield: 140 mg (70%). ^{1}H NMR (400 MHz, $CDCl_3$) δ 8.03 (d, J = 8.6 Hz, 2H), 7.89 (d, J = 8.7 Hz, 2H), 7.77 –7.73 (m, 6H), 7.68 (d, J = 8.7 Hz, 2H). ^{13}C NMR (100.3 MHz, $CDCl_3$) δ 152.5, 152.1, 144.7, 141.9, 138.6, 132.9, 128.2, 128.0, 124.7, 123.9, 118.9, 111.7, 98.3. ESI MS (*m/z*) calculated for $[C_{19}H_{12}IN_3H]^+$ 410.02, found: 410.29.

(*E*)-4'-((4-(4,4,5,5-tetramethyl-1,3,2-dioxaborolan-2-yl)phenyl)diazenyl)-[1,1'-biphenyl]-4-carbonitrile (5). A solution of **4** (150 mg, 0.12 mmol), KOAc (35.3 mg, 0.36 mmol, 3 eq.), bis(pinacolato)diboron (138 mg, 0.18 mmol, 1.5 eq.) and a catalytic amount of $Pd(dppf)Cl_2$ (3.5 mg) in dry and degassed dioxane (3 mL) was stirred at 80 ^{o}C overnight. The solution was cooled down, diluted with dichloromethane and washed with water, then dried over $MgSO_4$, filtered and concentrated. The residue was purified by chromatography in toluene-hexane 9:1 → toluene-MeOH 99:1 to give **5** as an orange solid. Yield: 75 mg (50%). ^{1}H NMR (400 MHz, $CDCl_3$) δ 8.04 (d, J = 8.6 Hz, 2H), 7.98 (d, J = 8.4 Hz, 2H), 7.92 (d, J = 8.4 Hz, 2H), 7.76 (m, 6H), 1.38 (s, 12H). ^{13}C NMR (100.3 MHz, $CDCl_3$) δ 154.5, 152.7, 144.7, 141.7, 135.8, 132.9, 128.2, 128.0, 123.9, 122.2, 118.9, 111.6, 84.3, 25.1. ESI MS (*m/z*) calculated for $[C_{25}H_{24}BN_3O_2H]^+$ 410.20, found: 410.08.

Compound 1 and **2.** A solution of **5** (60 mg, 0.15 mmol, 3 eq.), **6** (or **7**) (54 mg, 0.05 mmol), $Pd(PPh_3)_4$ (6 mg) and aqueous Na_2CO_3 (2 M, 5 mL) in THF (8 mL) was degassed and stirred under N_2 atmosphere at 80 ^{o}C for 48 h. The layers were separated and the aqueous phase was extracted with EtOAc. The combined organic layers were washed with water, dried ($MgSO_4$), filtered and concentrated. The residue was purified by chromatography in EtOAc-MeOH 24:1→ 23:2 to yield compound **1** (or **2**) as an orange solid. Yield: 56 mg (74%) for **1** and 47 mg (62%) for **2**.

(**1**) ^{1}H NMR (400 MHz, CD_3CN) δ 7.96 (dd, J = 8.6, 1.8 Hz, 8H), 7.90 – 7.76 (m, 16H), 7.55 (s, 1H), 7.25 (d, J = 1.4 Hz, 2H), 4.19 (d, J = 5.7 Hz, 2H), 3.60 – 3.27 (m, 64H), 3.24 (s, 12H), 2.36 (dt, J = 11.7, 5.9 Hz, 1H), 1.00 (d, J = 6.3 Hz, 12H). ^{13}C NMR (100.3 MHz, CD_3CN) δ 161.1, 153.3, 152.8, 145.0, 144.3, 142.7, 142.3, 133.8, 129.1, 129.0, 128.7, 124.3, 124.3, 114.0, 112.2, 75.6, 75.5, 72.6, 71.4, 71.1, 71.0, 70.2, 69.9, 68.0, 58.9, 42.0, 17.4. HR-MS (*m/z*) calculated for $[C_{88}H_{116}N_6O_{19}H]^+$ 1560.8295, found 1560.8214.

(**2**) ^{1}H NMR (400 MHz, CD_3CN) δ 8.03 (dd, J = 8.6, 1.6 Hz, 8H), 7.94 (d, J = 8.6 Hz, 4H), 7.90 – 7.83 (m, 12H), 7.63 (t, J = 1.4 Hz, 1H), 7.32 (d, J = 1.4 Hz, 2H), 4.23 (d, J = 5.6 Hz, 2H), 3.58 – 3.54 (m, 4H), 3.51 – 3.40 (m, 64H), 3.25 (s, 12H), 2.38 (dt, J = 11.9, 5.9 Hz, 1H), 2.06 (dt, J = 11.8, 6.1 Hz, 2H). ^{13}C NMR (100.3 MHz, CD_3CN) δ 161.1, 153.3, 152.8, 144.9, 144.2, 142.7, 142.2, 133.7, 129.1, 129.0, 128.7, 124.3, 119.6, 119.2, 114.0, 112.2, 72.5, 71.3, 71.1, 71.0, 70.9, 70.1, 69.8, 67.3, 58.8, 41.2, 40.9. ESI MS (*m/z*) calculated for $[C_{84}H_{108}N_6O_{19}H]^+$ 1505.77, found: 1505.80.

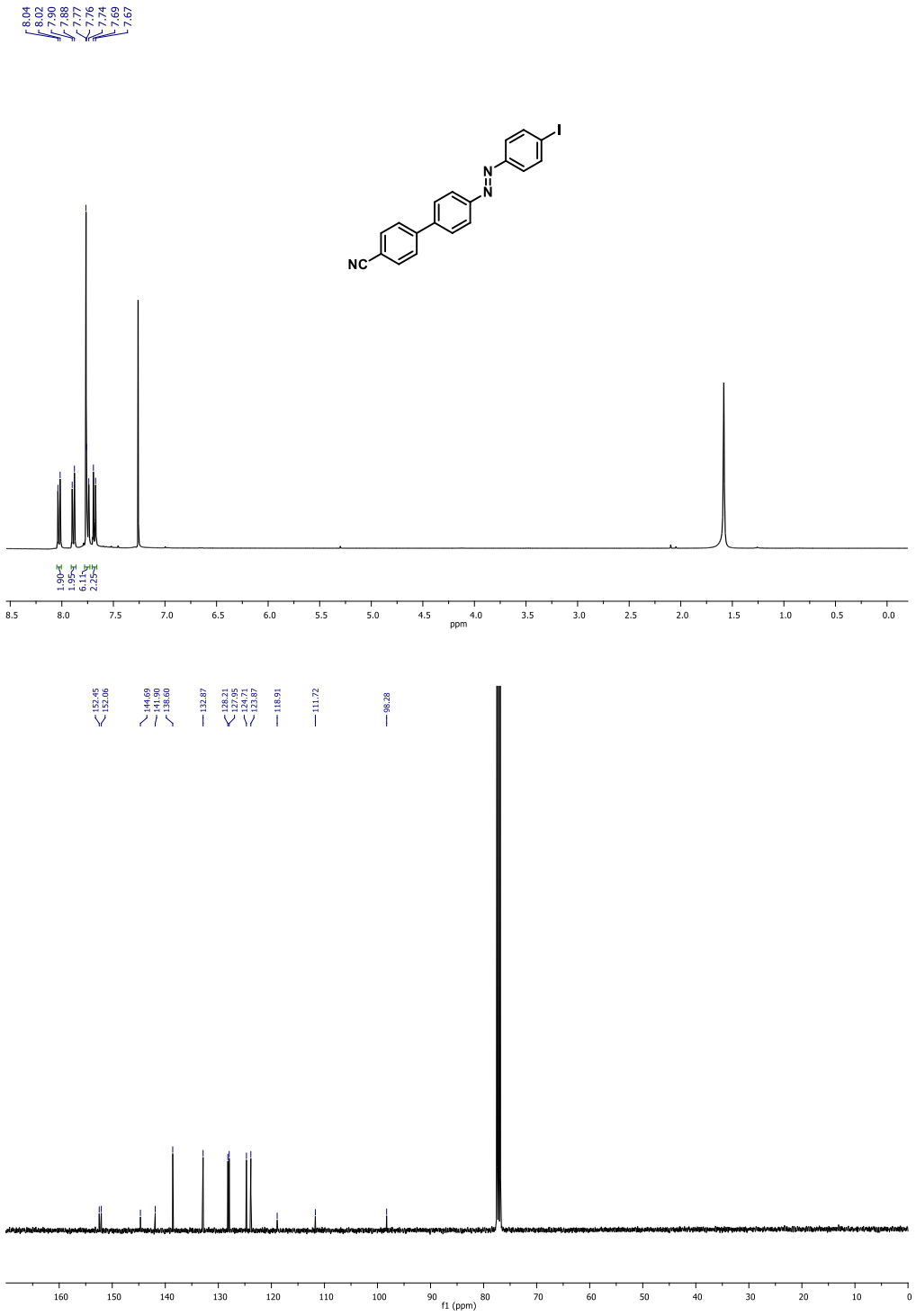

Figure S1. ^{1}H-NMR (top) and ^{13}C-NMR (bottom) spectra of compound 4 in $CDCl_3$.

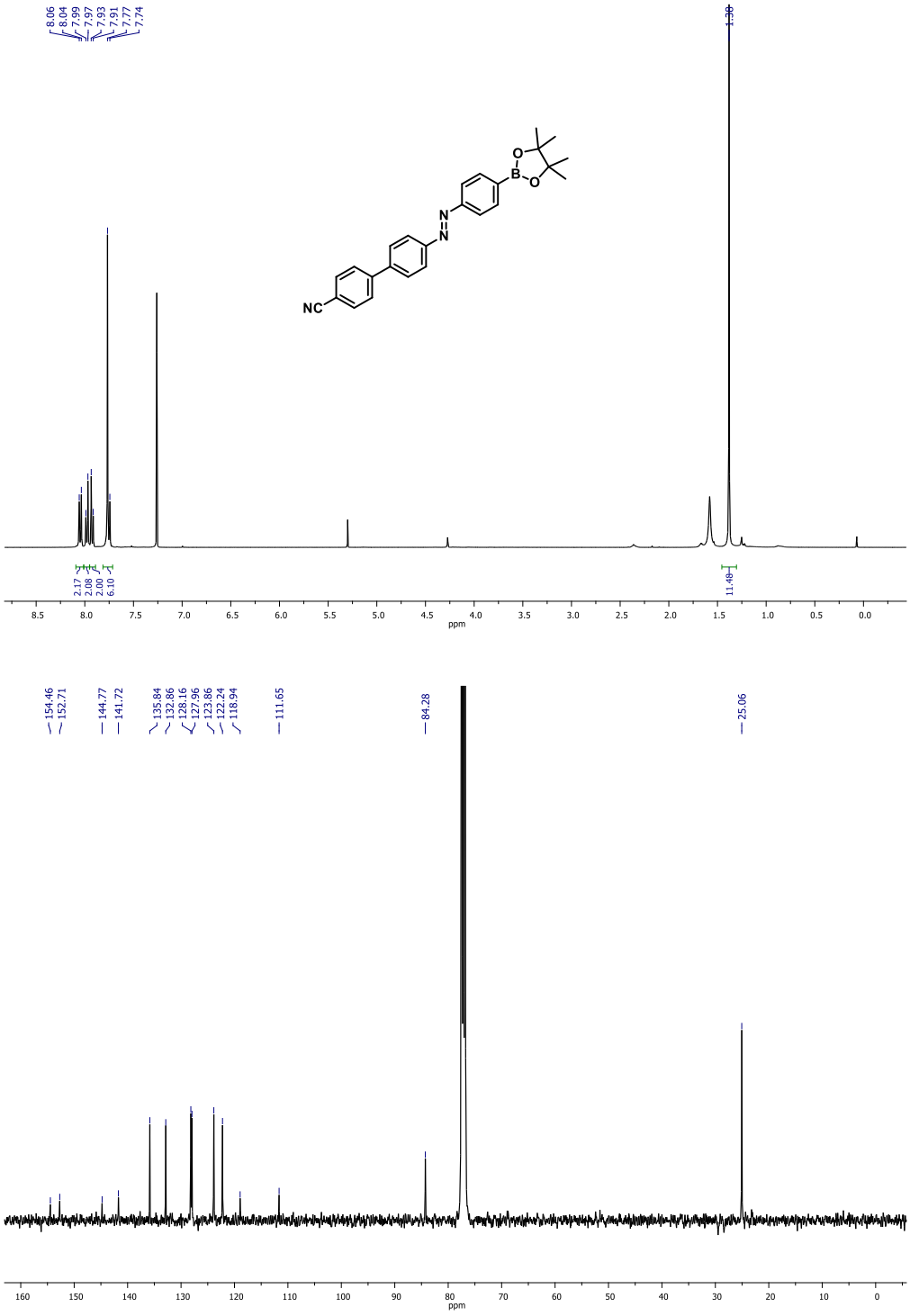

Figure S2. ^{1}H-NMR (top) and ^{13}C-NMR (bottom) spectra of compound 5 in $CDCl_3$.

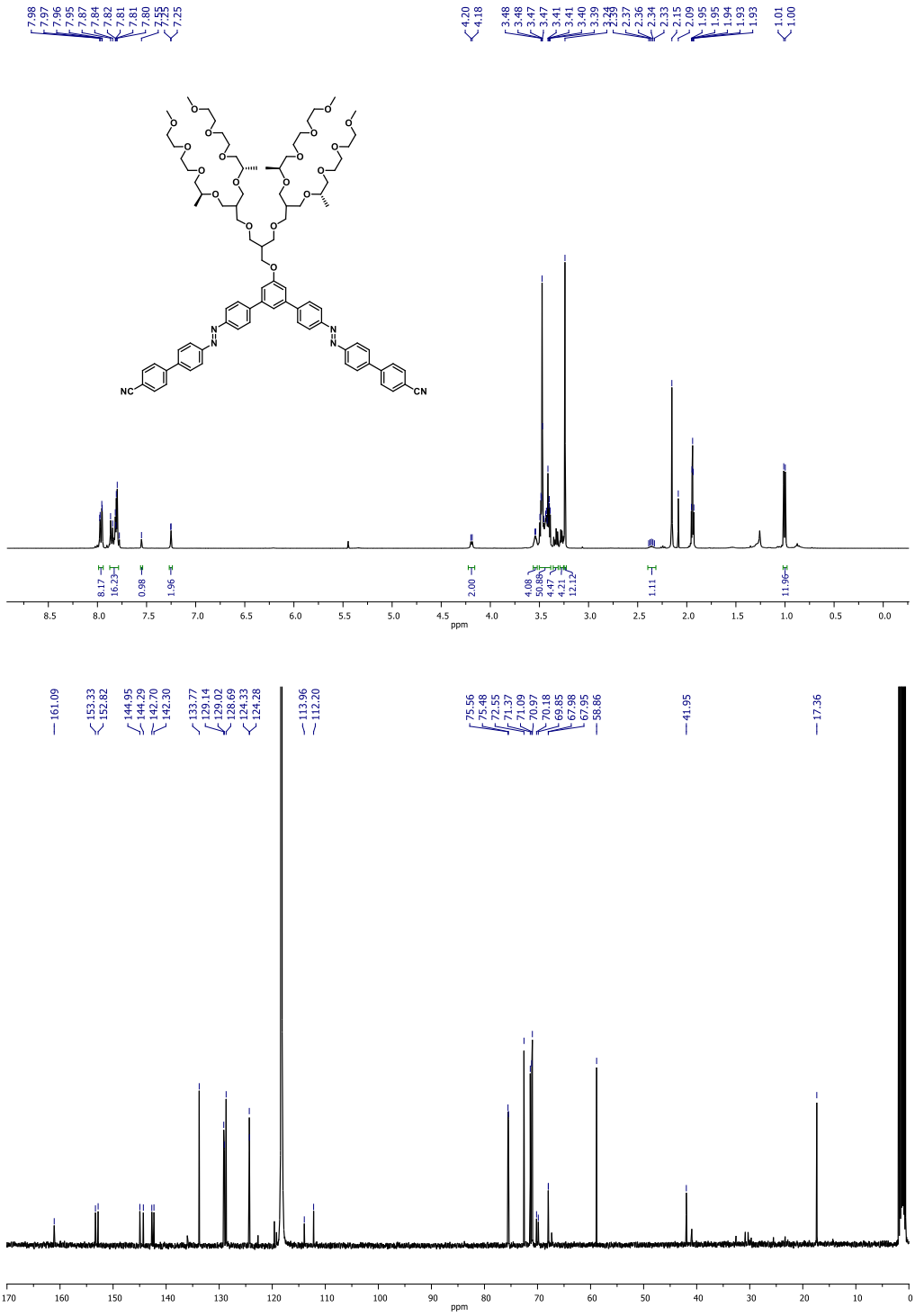

Figure S3. ^{1}H-NMR (top) and ^{13}C-NMR (bottom) spectra of compound 1 in MeCN-d$_3$.

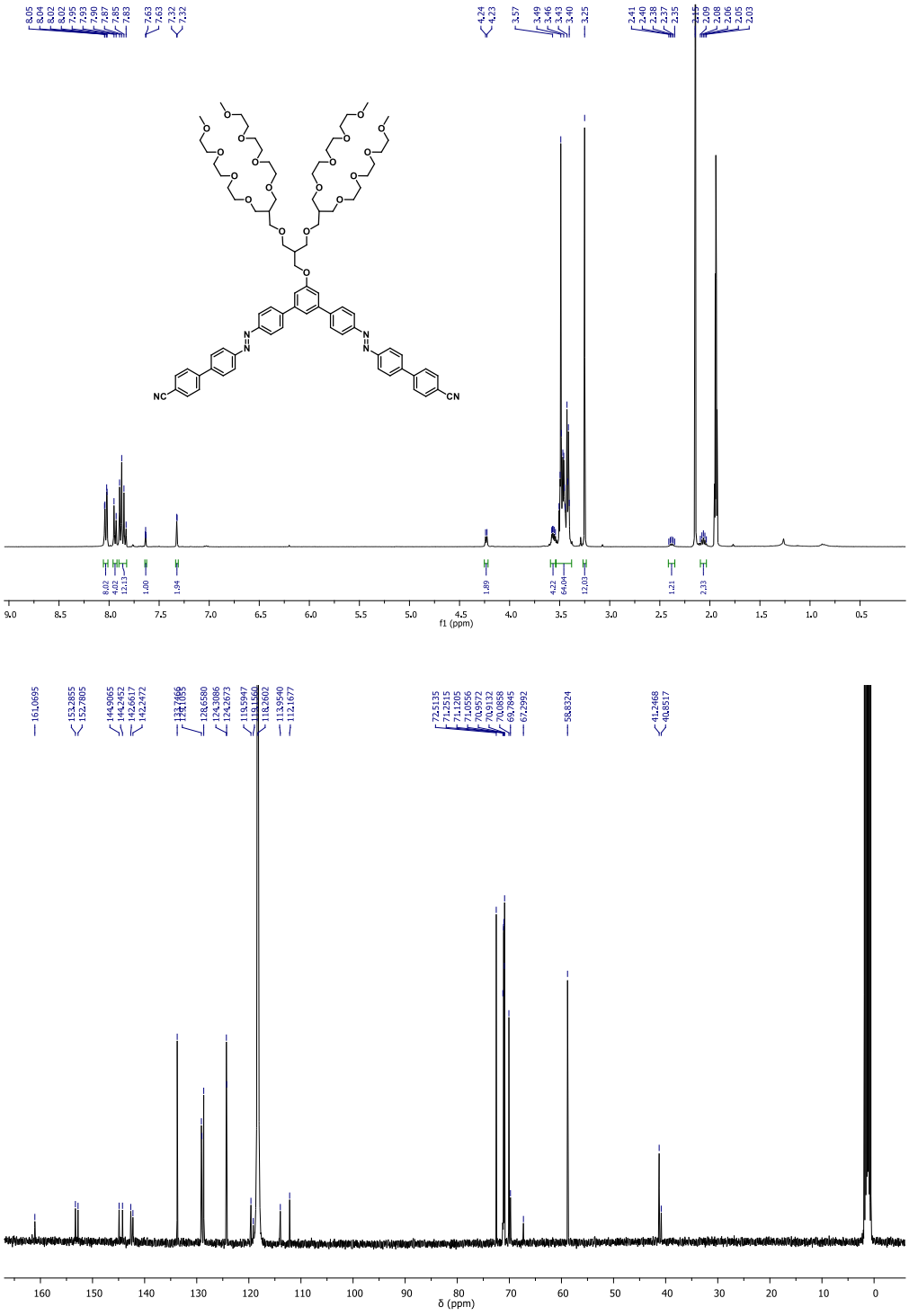

Figure S4. ^{1}H-NMR (top) and ^{13}C-NMR (bottom) spectra of compound 2 in MeCN-d$_3$.

3. Supporting experimental figures

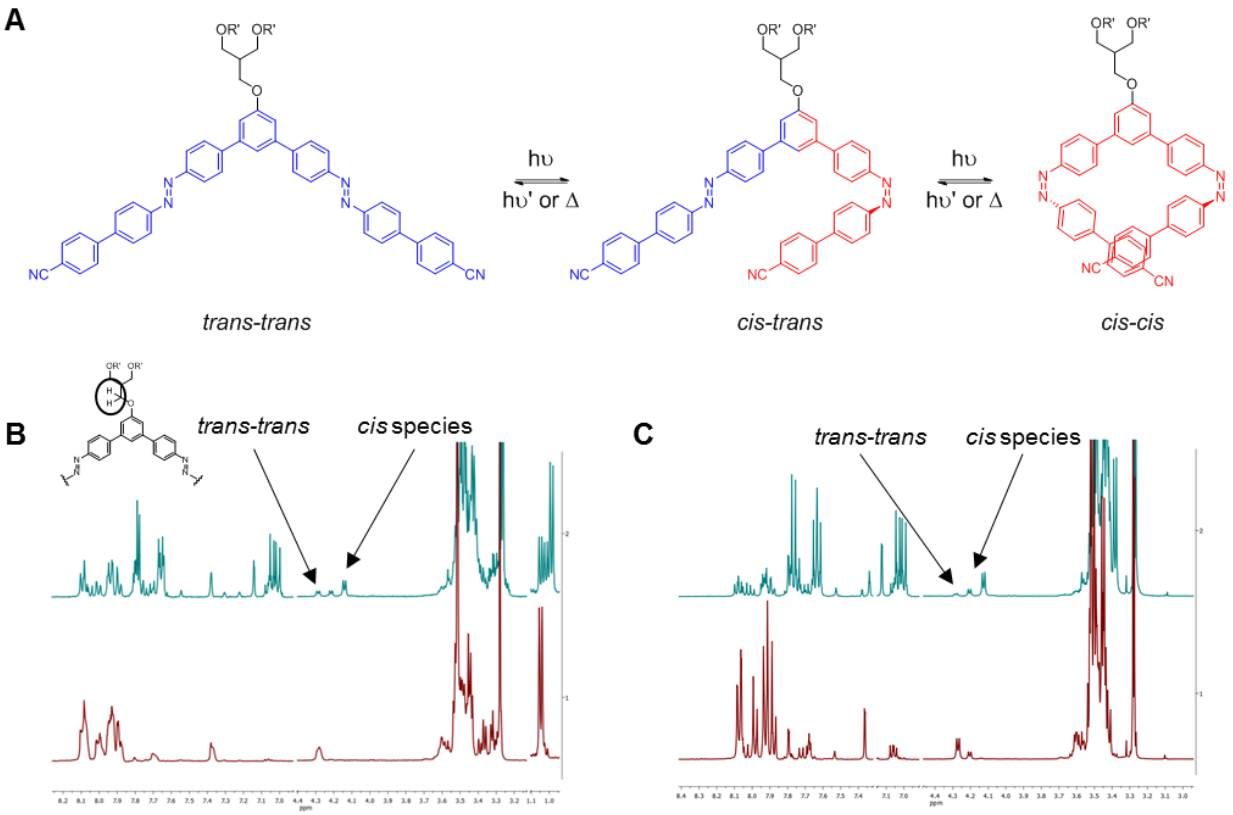

D

Compound	*Ratio switch trans/cis form*
1	39/61
2	29/71

Figure S5. Determination of the photo-stationary state in acetonitrile by ^{1}H-NMR. (A) Azobenzenes compound states. Upon UV irradiation the initial *trans-trans* azobenzene switches to the *cis-trans* and *cis-cis* forms. (B) ^{1}H-NMR (400 MHz in CD_3CN) spectra of chiral compound **1** and (C) achiral compound **2** at the initial state (red spectra) and after UV light irradiation (λ = 365 nm, green spectra). (D) Ratio of the ^{1}H-NMR of the integrated peaks (highlighted by the arrows) corresponding to the *trans*/*cis* signals of compounds **1** and **2**. The smaller proportion of the *cis* isomer in the case of compound **1** is probably due to the fact that the photostationary state was not reached at that moment. Irreversible photo-degradation became more prominent and have not allowed us to analysis the NMR spectra unambiguously.

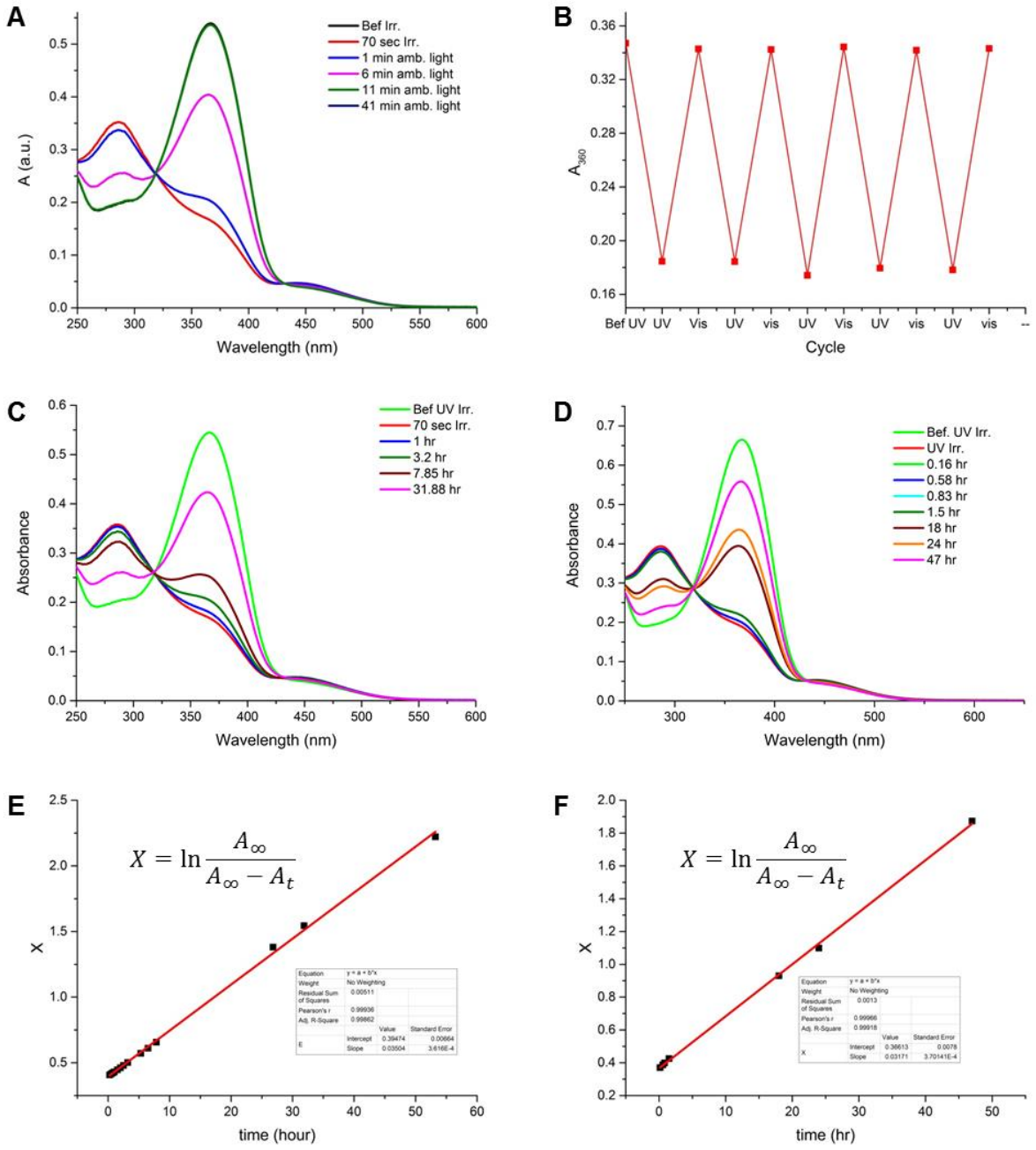

Figure S6. UV-vis spectra of the isolated single building blocks 1 and 2 in acetonitrile. (A) After UV irradiation and relaxation under ambient light for the chiral compound **1**. (B) Cycles of UV irradiation (λ = 365 nm, 15 s) and relaxation with the ambient light for the chiral compound **1**. (C) UV-vis spectra of thermal relaxation of the chiral azobenzene **1** and (D) achiral azobenzene **2** in dark. (E) and (F) Linear fitting of the relaxation for azobenzenes **1** and **2** taking into account the reversibility of the reaction due to the low intensity of the UV light. The law rate is $\boldsymbol{v} = \boldsymbol{k_1}[\boldsymbol{cis}] - \boldsymbol{k_2}[\boldsymbol{trans}]$. A_∞ is the absorption at the initial state at 360 nm and A_t the absorbance at the time *t* at 360 nm

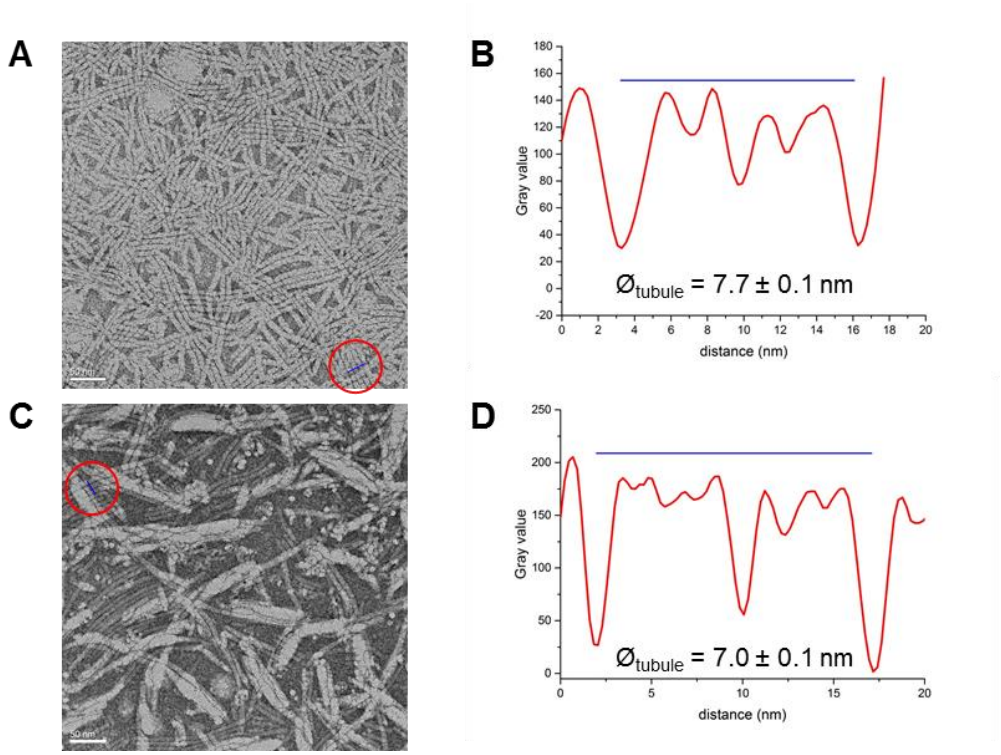

Figure S7. TEM micrographs of the tubules. (A) TEM of the tubules with the chiral building block **1** (83µM). (B) Grey value profile of an area of TEM picture a. (C) TEM of the tubules with the achiral building block **2** (80 µM). (D) Grey value profile of an area of the TEM picture C.

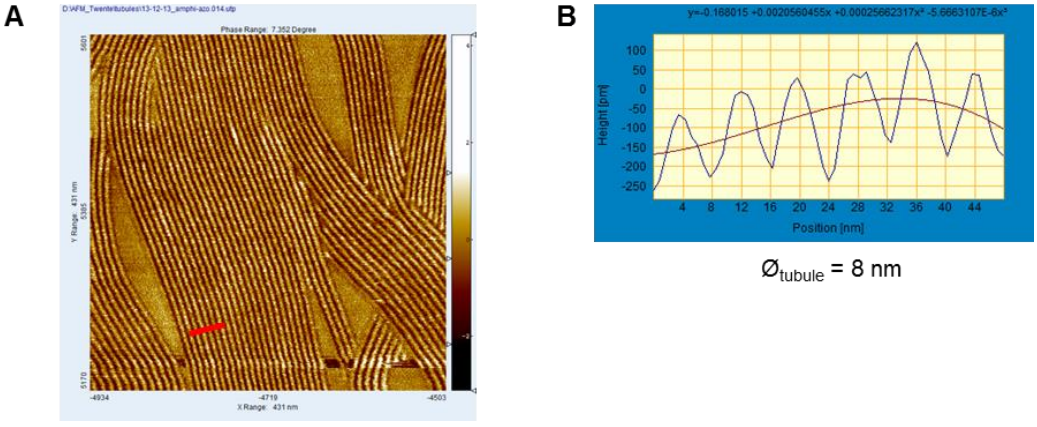

Figure S8. AFM visualization of the tubules. (A) AFM phase image of the synthetic tubules self-assembled from the achiral building block **2** in water and deposited on mica. (B) Height profile from the AFM image.

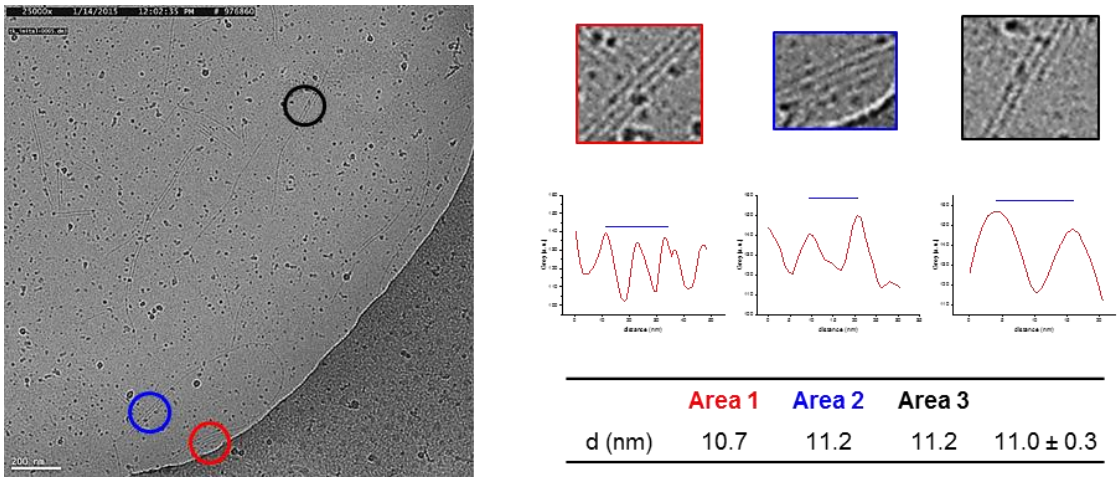

Figure S9. Measurements of the external diameter from the periodicity of the bundled tubes 2 (1.33 mM) observed by Cryo-TEM. External diameter of the tubules was measured at 3 different areas and subsequently averaged.

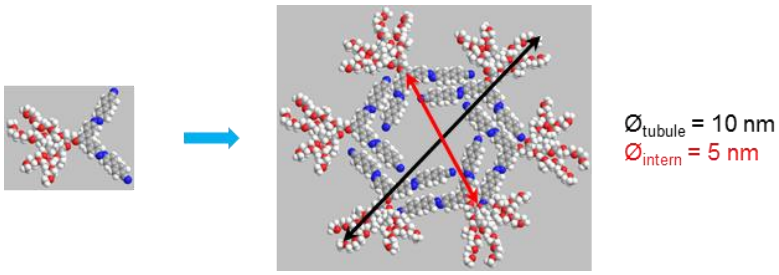

Figure S10. 3D model of the tentative hexameric non-covalent macrocycle composing the tubules with the characteristic diameters (Chem3D®).

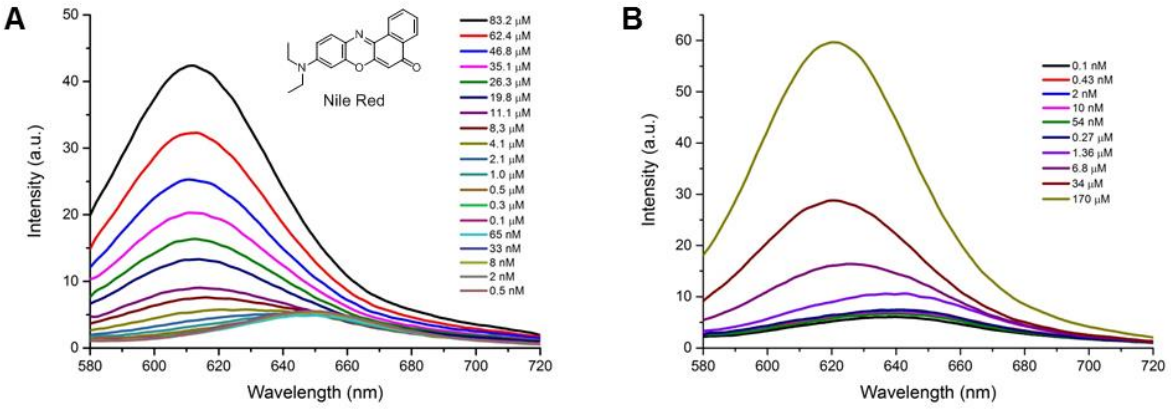

Figure S11. Determination of the critical aggregation concentration. Emission spectra of Nile Red solution (0.94 µM) in water with different concentration of (A) chiral azobenzene **1** and (B) achiral azobenzene **2**.

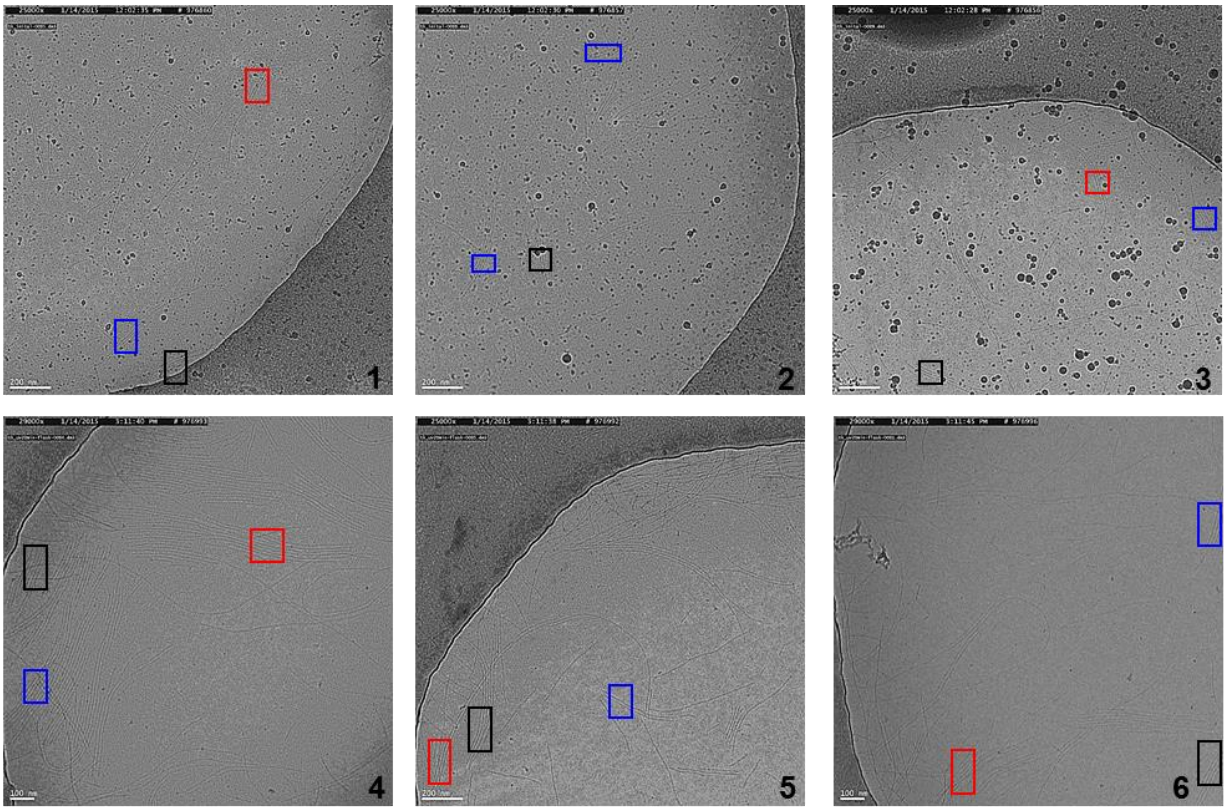

Before UV irradiation

Picture	Area 1	Area 2	Area 3	Average
1	10.7	11.2	11.2	**11.0**
2	12.9	12.9	12.1	**12.7**
3	12.0	12.0	10.6	**11.6**
			Average	**11.8 ± 0.8**

20 min irradiation

Picture	Area 1	Area 2	Area 3	Average
4	12.2	13.0	13.2	**12.8**
5	13.9	14.8	12.1	**13.6**
6	13.4	14.9	13.0	**13.8**
			Average	**13.4 ± 0.5**

Figure S12. Modification of the diameters of the tubules 2 (1.33 mM) before and after 20 minutes of UV light irradiation. The measurements have been done by using the difference of the contrast on pictures at different areas of bundled tubules. Values are given in nm.

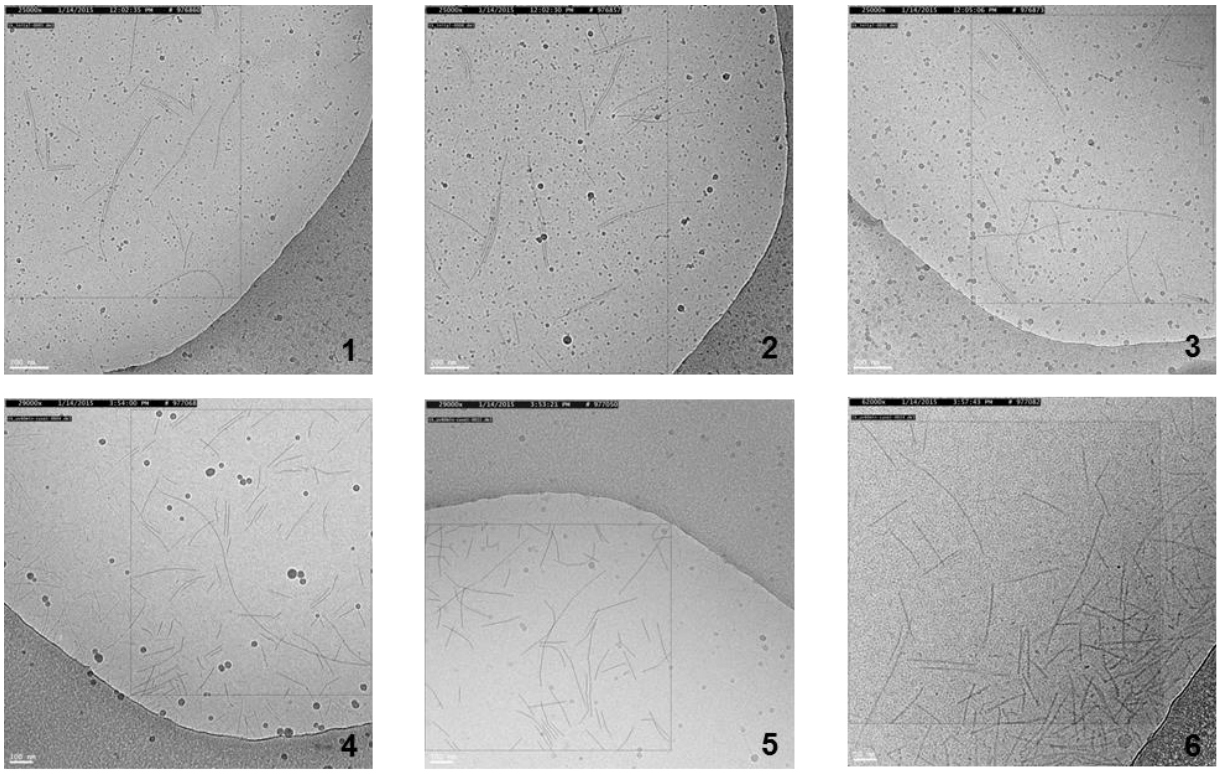

Before UV irradiation

Picture	Number of tubules
1	17
2	17
3	15
Average	**16 ± 1**

60 min irradiation

Picture	Number of tubules
4	67
5	154
6	57
Average	**93 ± 53**

Figure S13. Comparison of the number of the tubules 2 (1.33 mM) before and after 60 minutes of UV light irradiation.

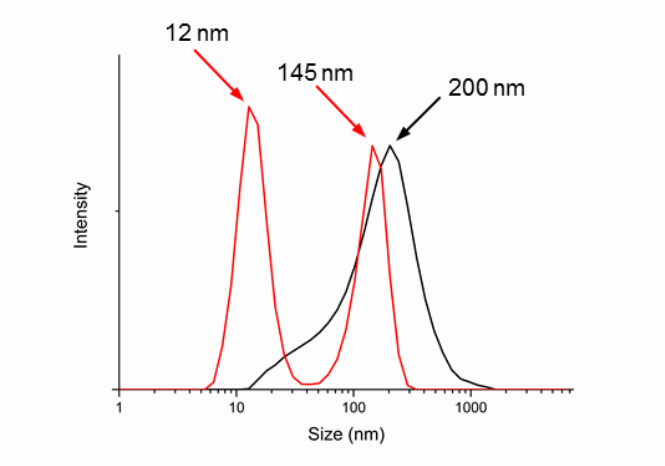

Figure S14. Dynamic light scattering measurements of the size of the tubules formed by compound 2 in water before and after UV irradiation. The concentration of the solution was 100 μM. Black line – before UV light irradiation and red line – after UV light irradiation for 100 min.

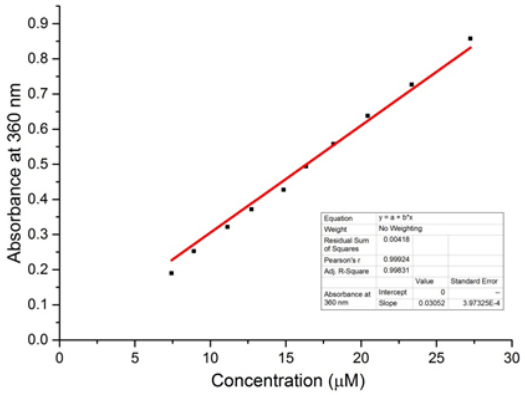

ε (L.mol^{-1}.cm^{-1})	*trans* (μM)	*cis* (μM)	Ratio *trans*/*cis* (%)
30520	1.9	0.4	83/17

Figure S15. Estimation of the *trans/cis* ratio during the UV irradiation process at 35 min. From the calibration curve of the absorption at 360 nm (30520 L.mol^{-1}.cm^{-1}, *cis* form has negligible absorption at this wavelength) at changing concentration of the compound **1** in water, the amount of the *trans* form was estimated to be 83 %.

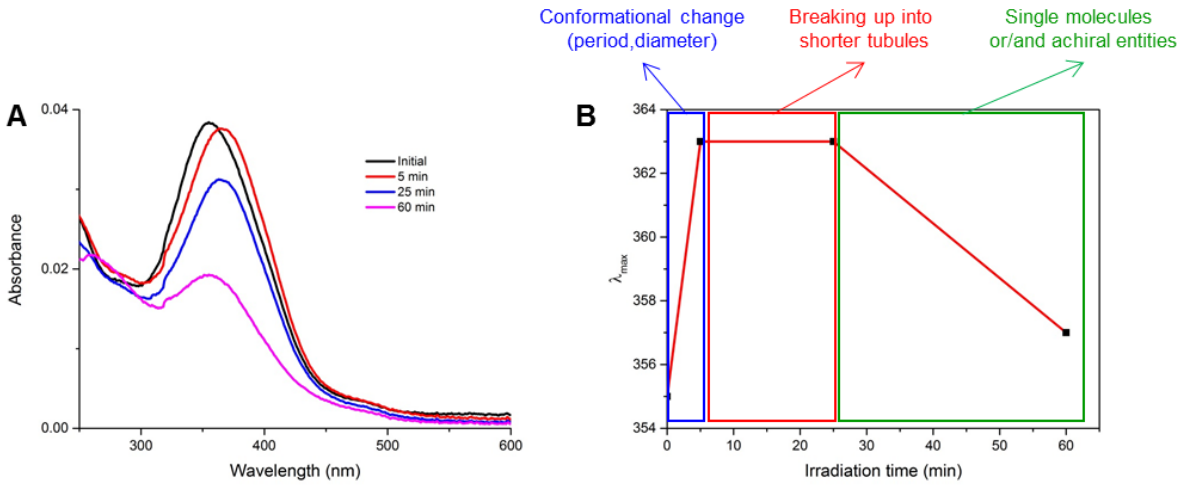

Figure S16. Observation of the 3 step disassembly process of the tubules by UV-vis for the achiral building block 2 in water. (A) UV-vis spectra upon UV irradiation. (B) λ_{max} *versus* irradiation time and the 3 observed steps. As observed for the tubule formed by chiral building block **1**, a red shift appeared at the initial state showing that the structure of the tubules is changing. In the second step the λ_{max} remains constant while the tubules break up into shorter fragments. Finally, the fully disassembly is accompanied by the blue shift of the λ_{max}.

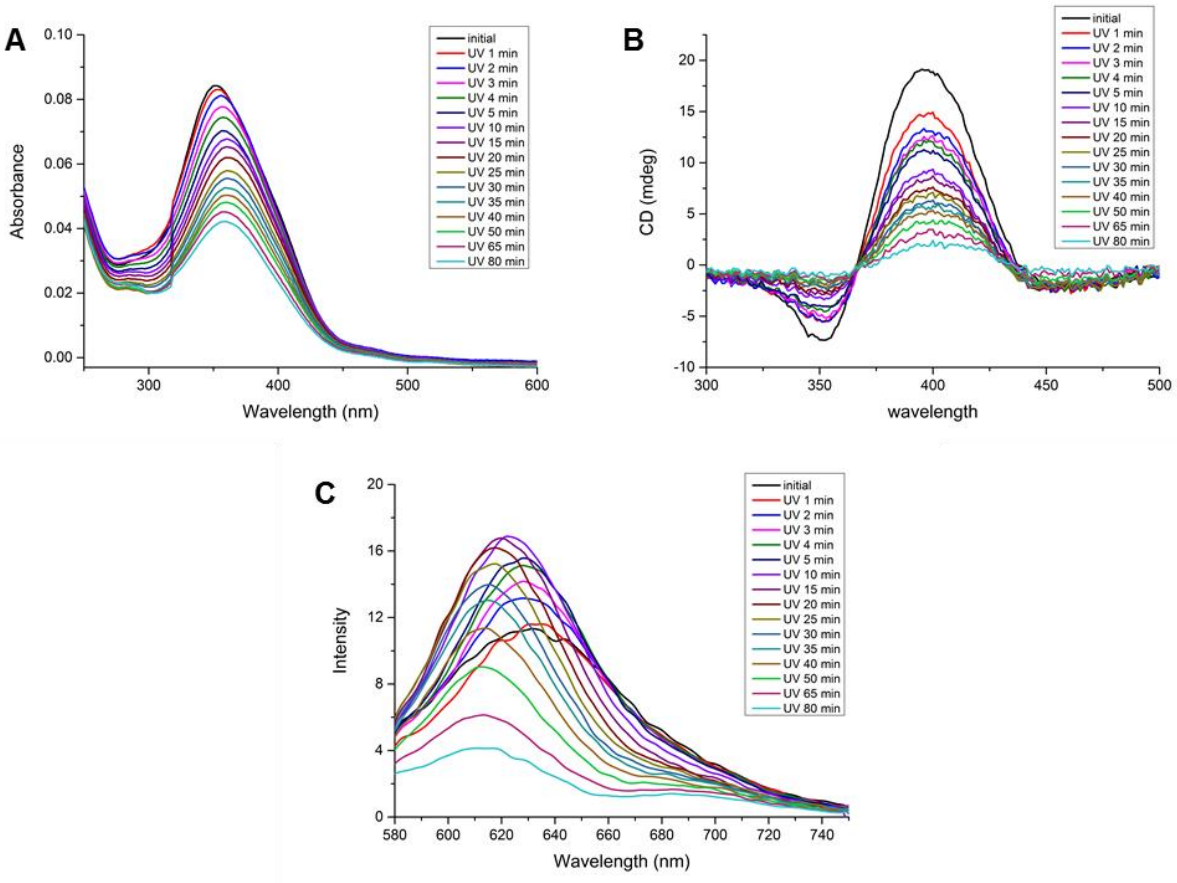

Figure S17. Photo-triggered disassembly of tubules formed by compound 1 (2.5 μM) in water with encapsulated Nile Red (0.94 μM). (A) UV-vis, (B) CD and (C) fluorescent spectra upon UV irradiation.

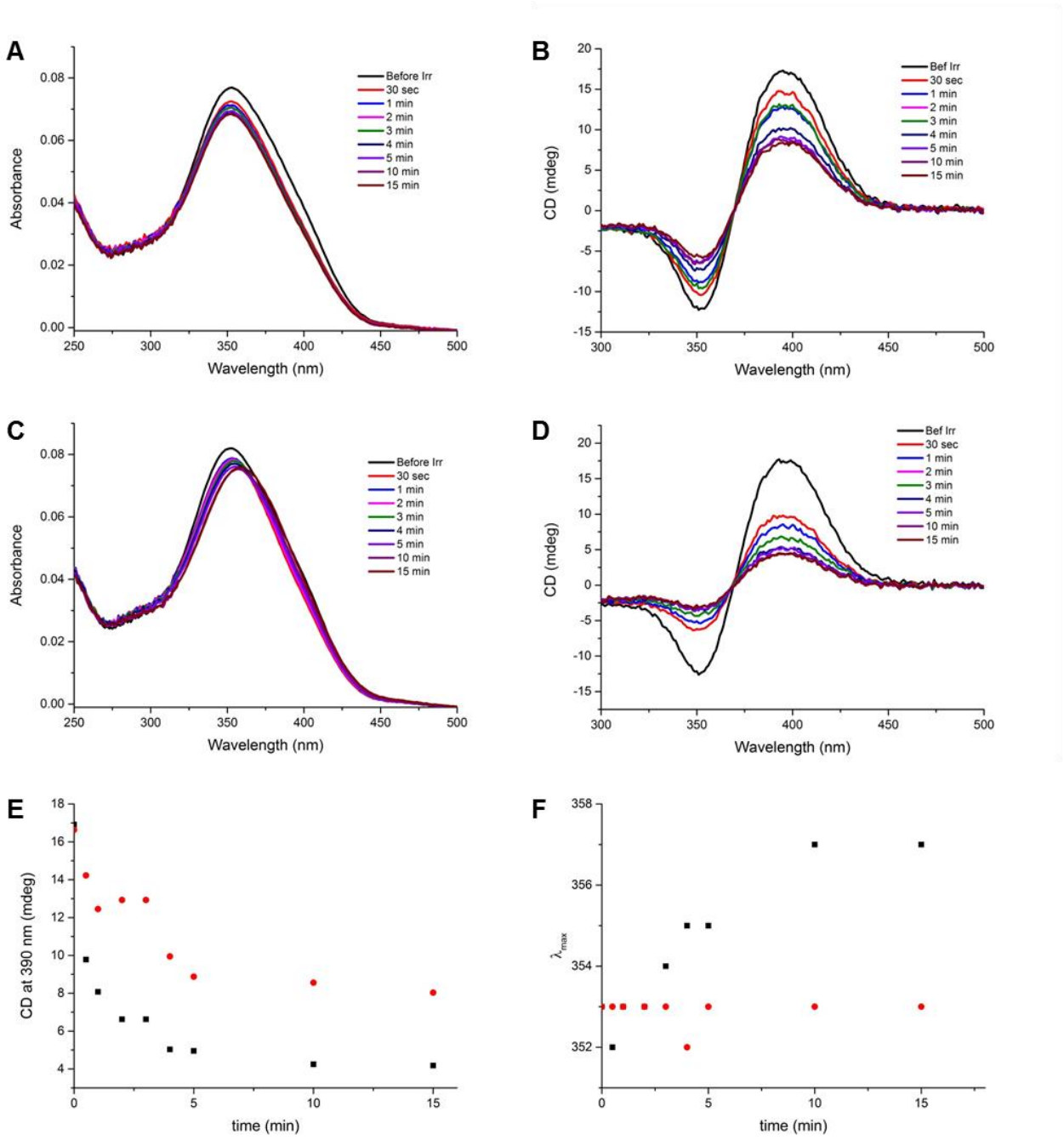

Figure S18. Comparison of the initial state of the disassembly process in pure water and water/acetonitrile mixture (95/5). (A) UV-vis and (B) CD spectra of a solution of the tubules formed by **1** at 2.5 μM in water/acetonitrile mixture (95/5) upon UV irradiation. (C) UV-vis and (D) CD spectra of a solution of tubules formed by **1** at 2.5 μM in water upon UV irradiation. (E) CD signal at 390 nm and (F) UV-vis λ_{max} shifts *vs* irradiation time in water (black dots) and in water/acetonitrile mixture (red dots).

4. Computational methods

Construction of the atomistic models and equilibration AA-MD simulations. The atomistic (AA) models for monomer **1** and supramolecular tubule **1** were built and parametrized according the procedure recently adopted for similar self-assembling motifs (5-9). In particular, the AA model of monomer **1** was parametrized based on the General Amber Force Field, GAFF (*gaff.dat*) (10). The initial structure of tubule **1** was built starting from eleven hexagonal macrocycles, each containing six monomers **1** (Fig. 1a), which have been stacked on the top of each other along *z*-direction (initial stacking distance of 4.4 Å) with a mutual tilting angle of 16.4°. Such a starting configuration for tubule is consistent with recent literature report on a similar tubule (11). This tubule portion (composed of 66 monomers) was inserted into a simulation box (initial $X \times Y \times Z$ dimensions of 12 × 12 × 4.84 nm) grazing the tube in *z*-direction and filled of explicit TIP3P (12) water molecules. In this way, replicated along *z* via periodic boundary conditions, this system effectively modeled a portion of the bulk of an infinite (helical) tubule **1**.

All simulations were conducted with the GROMACS 5.1.2 software (13). After initial minimization, tubule **1** was equilibrated for 150 ns of AA-MD in periodic boundary NPT (constant N: number of atoms, P: pressure and T: temperature) using a timestep of 2 fs and a 10 Å cutoff. This simulation time was sufficient for the tubule to reach stable structural and energetic equilibration in the AA-MD regime (Fig. S15). All AA-MD runs were conducted at 300 K (27°C) using the v-rescale (14) thermostat (coupling constant of 2.0 ps) and 1 atm of pressure using semi-isotropic pressure scaling (compatibly with the directional nature of the tubule) with coupling constant of 2 ps. The particle mesh Ewald (PME)(15) approach was used to treat long-range electrostatics. The LINCS algorithm was used to constrain all bonds involving hydrogens (16).

Well-tempered metadynamics simulations. The WT-MetaD (17) simulations have been conducted using the GROMACS 5.1.2 software (13) and the PLUMED 2 plugin (18). We used the C-N=N-C dihedral angle in the azobenzene tail of monomer **1** as the collective variable (CV) describing/biasing the *trans-cis* transition. In the WT-MetaD runs, we used a HILLS height of 0.28 kcal mol^{-1} and Gaussian SIGMA of 0.35 rad. A bias factor of 10 or 40 was used for the WT-MetaD simulations of the *trans-cis* transition in monomer **1** as respectively disassembled (in water) or assembled in the tubule. The other simulation parameters are the same reported above. From the WT-MetaD simulations we obtained the free-energy profiles for the *trans-cis* transition of the azobenzene groups in monomer **1** as disassembled in water or assembled in the tubule (Fig. S16a: black and red respectively). The transition requires more energy in the assembled state compared to the disassembled one due to the crowding present in the assembly (at least ~20 kcal mol^{-1} for an assembled monomer *vs.* ~9 kcal mol^{-1} for a disassembled one). In the experiments, light irradiation provides the energy necessary to this transition. We used this information to set up out-of-equilibrium AA-MD simulations where *trans-cis* transitions in the tubule could be monitored iteratively.

Out-of-equilibrium AA-MD simulations and analysis of strain build-up. We modified the native dihedral angle potential of the azobenzene groups in monomer **1** to observe spontaneous trans-cis transitions during an AA-MD run (Fig. S16b). This is equivalent to adding a static bias to the azobenzene dihedral potential of the monomers in tubule **1**. In the equilibrium AA-MD, the C-N=N-C dihedral potential of the native azobenzene groups in monomer **1** was defined by the sum of two terms as in Eq. S1 (standard for this group in the GAFF force field):

$$V_{d,native}(\varphi) = k_1\left(1 + \cos\left(n_1\varphi - \varphi_{1,s}\right)\right) + k_2\left(1 + \cos\left(n_2\varphi - \varphi_{2,s}\right)\right) \quad \text{(S1)}$$

where k_1 = 3 kcal mol^{-1}, n_1 = 2, $\varphi_{1,s}$ = 180° and k_2 = 2.8 kcal mol^{-1}, n_2 = 1, $\varphi_{2,s}$ = 0° (Fig. S16b: black curve). In the out-of-equilibrium AA-MD runs, such dihedral potential was modified as in Eq. S2 for all monomers in tubule **1**:

$$V_{d,out-of-equil}(\varphi) = k_3\left(1 + \cos\left(n_3\varphi - \varphi_{3,s}\right)\right) \quad \text{(S2)}$$

where k_3 = 6.2 kcal mol^{-1}, n_3 = 1, $\varphi_{3,s}$ = 180° (Fig. S16b: red curve). This moved the *trans* configuration of the monomers in pre-equilibrated tubule **1** out-of-equilibrium, favoring transition to *cis* inside the tubule. The parameters of Eq. S2 were optimized to obtain a bias on the azobenzene dihedral potential consistent with the energy necessary for the *trans-cis* transition in an assembled monomer captured by WT-MetaD (~20 kcal mol^{-1}). This was verified to be the minimum bias to guarantee sufficient speed-up to allow us monitoring the *trans-cis* transitions in the timescale of the AA-MD run.

All other simulation parameters in these AA-MD runs were the same used for the equilibration runs (see above). During these out-of-equilibrium AA-MD simulations we monitored the *trans-cis* transitions of the azobenzene groups in the tubule using *gmx_angle*. The average energy absorbed by each assembled monomer in the tubule as a function of the percentage of *trans-cis* transitions (Fig. 7b: strain build-up) was calculated as: $\Delta E = E_{\text{perturbed}} - E_{\text{native}}$, where E_{native} is the average energy of the monomers in the unperturbed equilibrated tubule **1**, while $E_{\text{perturbed}}$ is the average energy of the (modified) monomers during the out-of-equilibrium AA-MD ($\Delta E > 0$ identifies unfavorable energy variation/accumulation). The $\Delta\Phi$ parameter (Fig. 7c: defined as $\Delta\Phi = \Phi_{\text{perturbed}} - \Phi_{\text{native}}$) measures the deviation during the runs from the parallel orientation of the planes defined by the aromatic rings in the monomers in equilibrated tubule **1** (stacking destabilization). The Φ parameter was calculated using the PLUMED plugin. $\Delta\Phi = 0$ means that the initial stacked configuration is perfectly preserved during the run, while the higher the $\Delta\Phi$, the higher the structural distortions in the assembly. All reported data were calculated as the average of three out-of-equilibrium runs.

5. Additional data from AA-MD simulations

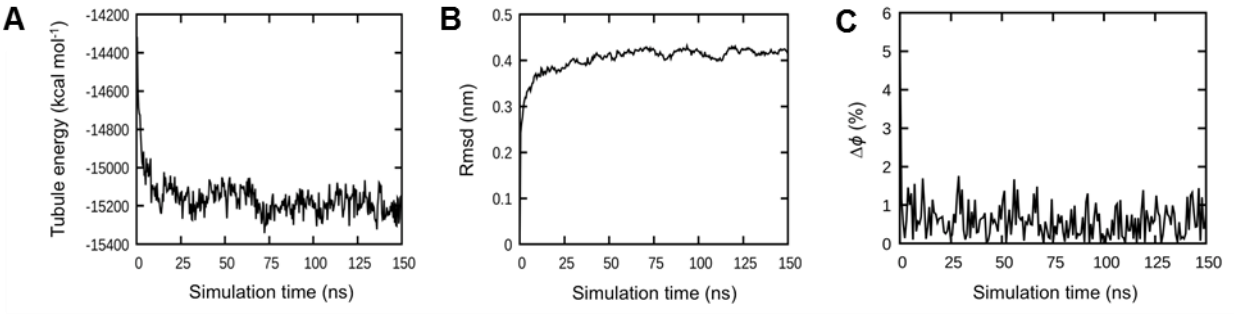

Figure S19. AA-MD equilibration of tubule 1. (A) Energy of tubule **1** as a function of AA-MD simulation time. (B) Root mean square deviation (Rmsd) of the atoms of tubule **1** as a function of AA-MD simulation time. (C) Deviation (in percentage) in the order parameter ($\Delta\Phi$) as a function of simulation time calculated respect to the ordered assembly of the monomers in equilibrated tubule **1**. All data show that tubule **1** reaches stable equilibration along the AA-MD run.

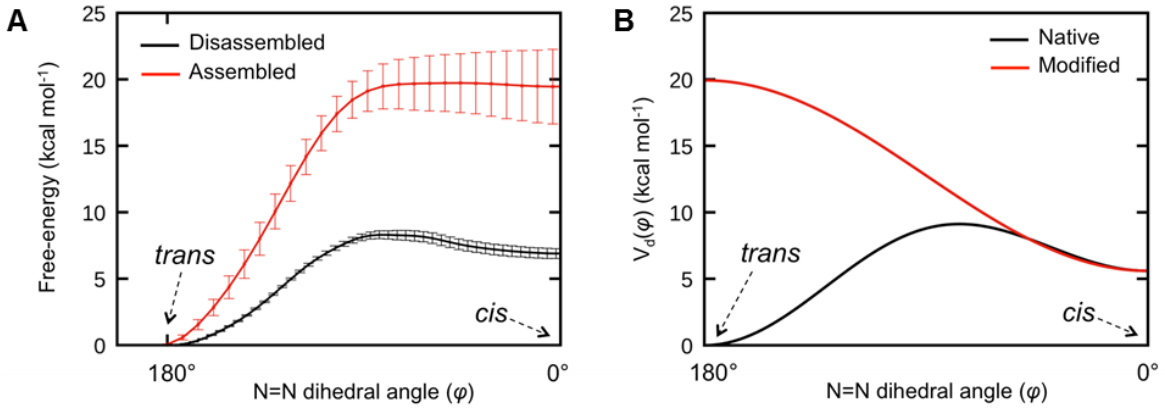

Figure S20. Azobenzene *trans-cis* transition in monomer 1. (A) Free-energy profiles for *trans-cis* transition as captured by WT-MetaD simulations in disassembled in monomer **1** (black) or in monomer **1** as assembled in the tubule (red). (B) Dihedral potential term for the azobenzene *trans-cis* transition in monomer **1**. Black: original non-modified dihedral (GAFF force field, Eq. S1). Red: modified dihedral (see Eq. S2) used in the out-of-equilibrium AA-MD simulations.

5. References

1. Chen CJ, Liu GY, Liu XS, Li DD, Ji J (2012) Construction of photo-responsive micelles from azobenzene-modified hyperbranched polyphosphates and study of their reversible self-assembly and disassembly behaviours. *New J Chem* 36:694–701.
2. Molander GA, Cavalcanti LN (2012) Nitrosation of aryl and heteroaryltrifluoroborates with nitrosonium tetrafluoroborate. *J Org Chem* 77:4402–4413.
3. Kim HJ, Zin WC, Lee M (2004) Anion-directed self-assembly of coordination polymer into tunable secondary structure. *J Am Chem Soc* 126:7009–7014.
4. Park IS, *et al.* (2011) Designer nanorings with functional cavities from self-assembling β-sheet peptides. *Chem Asian J* 6:452–458.
5. Amado Torres D, Garzoni M, Subrahmanyam AV, Pavan GM, Thayumanavan S (2014) Protein-triggered supramolecular disassembly: insights based on variations in ligand location in amphiphilic dendrons. *J Am Chem Soc* 136:5385–5399.
6. Baker MB, et al. (2015) Consequences of chirality on the dynamics of a water-soluble supramolecular polymer. *Nature Commun* 6:6234.
7. Bochicchio D, Salvalaglio M, Pavan GM (2017) Into the dynamics of a supramolecular polymer at submolecular resolution. *Nature Commun* 8:147.
8. Garzoni M, et al. (2016) Effect of H-bonding on order amplification in the growth of a supramolecular polymer in water. *J Am Chem Soc* 138:13985–13995.
9. Beltran E, et al. (2015) Self-organization of star-shaped columnar liquid crystals with a coaxial nanophase segregation revealed by a combined experimental and simulation approach. *Chem Commun* 51:1811–1814.
10. Wang J, Wolf RM, Caldwell JW, Kollman PA, Case DA (2004) Development and testing of a general amber force field. *J Comput Chem* 25:1157–1174.
11. Kim H-J, et al. (2010) Self-dissociating tubules from helical stacking of noncovalent macrocycles. *Angew Chem Int Ed* 49:8471–8475.
12. Jorgensen WL, Chandrasekhar J, Madura JD, Impey RW, Klein ML (1983) Comparison of simple potential functions for simulating liquid water. *J Chem Phys* 79:926–935.
13. Abraham MJ, et al. (2015) GROMACS: High performance molecular simulations through multi-level parallelism from laptops to supercomputers. *SoftwareX* 1–2:19–25.
14. Bussi G, Donadio D, Parrinello M (2007) Canonical sampling through velocity rescaling. *J Chem Phys* 126:014101.
15. Darden T, York D, Pedersen L (1993) Particle mesh Ewald: An N·log(N) method for Ewald sums in large systems. *J Chem Phys* 98:10089–10092.
16. Hess B, Bekker H, Berendsen HJC, Fraaije JGEM (1997) LINCS: A linear constraint solver for molecular simulations. *J Comput Chem* 18:1463–1472.
17. Barducci A, Bussi G, Parrinello M (2008) Well-tempered metadynamics: a smoothly converging and tunable free-energy method. *Phys Rev Lett* 100:020603.
18. Tribello GA, Bonomi M, Branduardi D, Camilloni C, Bussi G (2014) PLUMED 2: New feathers for an old bird. *Comput Phys Commun* 185:604–613.